



# Static recrystallization behaviour of Ti-Nb microalloyed high-strength steel

by C-Y. Zhou\*, G-L. Wu\*, and X-B. Liu\*

## Synopsis

The static recrystallization behaviour of Ti-Nb microalloyed high-strength steel during hot deformation was studied by conducting double-hit hot compression experiments using a Gleeble-3500 thermomechanical simulator. The effects of deformation temperature, strain rate, strain, and initial austenite grain size on the static recrystallization fraction are discussed. The static recrystallization kinetics were modelled, and the results show that the static recrystallization fraction increased with deformation temperature, strain rate, and strain and interpass time. The static recrystallization activation energy  $Q_s$  was 326.05 kJ mol<sup>-1</sup>. Comparison of the experimental results and predicted results indicates that the effects of deformation parameters on the static recrystallization in multistage hot deformation are significant. The predicted results are in good agreement with the experimental results.

## Keywords

Ti-Nb microalloyed high-strength steel, static recrystallization, activation energy, kinetic model.

## Introduction

In hot-forming processes, complex microstructures are often induced by multiple hot deformation mechanisms (Zhang *et al.*, 2014; Liang *et al.*, 2015). The softening behaviour during hot processing has generated considerable interest because component properties are influenced significantly by the corresponding microstructural evolution (Wu *et al.*, 2010). It is well known that dynamic recrystallization (DRX); metadynamic recrystallization (MDRX), which occurs by the growth of DRX nuclei during intervals of deformation; and static recrystallization (SRX), which occurs by nucleation and growth during the intervals of deformation, can significantly alter the austenite grain size (Chen *et al.*, 2015. Chen, Sui, and Cui, 2014; Mao *et al.*, 2014). The long interpass times allow complete SRX to take place if the steel is being rolled above the interpass recrystallization stop temperature ( $T_{nr}$ ), *i.e.* in the absence of carbonitride precipitation (Siciliano, 2000). In recent research, microalloying technology coupled with new-generation thermomechanical control processing (NG-TMCP) has proved efficient in achieving the proper balance between strength, toughness, ductility, and formability by means of a suitable

combination of chemical composition and thermomechanical treatment parameters (Shukla *et al.*, 2012; Bandyopadhyay *et al.*, 2011). The alloying elements Nb, V, Ti are widely used in high-strength low-alloy (HSLA) steel to achieve the desired strength and toughness properties with solid-solution strengthening, precipitation hardening, grain refinement, and dislocation strengthening (Opiela, 2014; Chen and Yu, 2012). The wide applicability of alloying elements in HSLA steel is due to the fact that heat treatments are not required after forming of the parts, which results in time and cost savings.

When microalloying elements are added to steel, the dissolved alloying additions in solid solution raise the temperature of recrystallization of plastically deformed austenite. This is due to segregation on the dislocations and grain boundaries, causing a decrease in the recovery rate and grain boundary mobility (Ferdowsi *et al.*, 2014). Instead, alloying elements precipitating on dislocations in the form of dispersive carbides and/or carbonitrides slow the course of recrystallization during plastic deformation (Cabrera *et al.*, 1997; Mirzadeh, Cabrera, and Najafzadeh, 2012). The SRX behaviour depends on the processing parameters, such as strain rate, deformation temperature, and strain. A finer initial grain size accelerates recrystallization, and precipitation can retard recrystallization (Miao *et al.*, 2012). Therefore, in order to optimize the hot processing parameters, it is important to understand the characteristics of hot deformation to control the microstructure evolution. In this article, the SRX behaviour of Ti-Nb microalloyed high-strength steel during hot deformation was studied using a Gleeble-

\* School of Minerals Processing and Bioengineering, Central South University, China.

© The Southern African Institute of Mining and Metallurgy, 2017. ISSN 2225-6253. Paper received Sep. 2015; revised paper received Oct. 2016.

# Static recrystallization behaviour of Ti-Nb microalloyed high-strength steel

3500 thermomechanical simulator. The effects of deformation temperature, strain rate, strain, and initial austenite grain size on the SRX fraction are discussed and the SRX kinetics modelled, which will be helpful for optimizing the rolling process.

## Experimental

The chemical composition of the high-strength steel used in this investigation was 0.078C-0.25Si-1.78Mn-0.12Ti-0.035Nb-0.008P-0.003S-0.003Al-0.0038N (bal. Fe), in wt%. Cylindrical specimens were machined with a diameter of 8 mm and height of 12 mm. To prevent possible non-uniform temperature distribution in the sample, special cemented carbide products were fixed to both ends of the deformed sample. The uniaxial hot compression tests were conducted using a Gleeble-3500 thermomechanical simulator. In order to determine the critical strain for the start of DRX, the hot compression tests were performed in the temperatures range of 950–1050°C, at intervals of 50°C, under constant strain rates of 0.1, 1, and 5 s<sup>-1</sup>, up to a true strain of 0.9. Double-hit tests were performed to study the progress of SRX. As shown in Figure 1, the specimens were heated to 1200°C at a heating rate of 10°Cs<sup>-1</sup> and held at temperature for 5 minutes. The specimens were then cooled to the deformation temperature at 10°Cs<sup>-1</sup> and held for 1 minute to eliminate thermal gradients. Temperatures of 950, 1000, and 1050°C, strain rates of 0.1, 1, and 5 s<sup>-1</sup>, strains of 0.10, 0.15, and 0.20, and interval times between the two deformation passes of 1, 5, 10, 30, and 100 seconds were used. In order to research the effect of initial austenite grain sizes on SRX, the specimens were heated to 1200°C and held for different times to obtain different initial austenite grain sizes.

Optical metallographic samples were prepared by conventional grinding and polishing techniques, and were subsequently etched with saturated aqueous picric acid solution and sodium dodecyl benzene sulphonate for 200 seconds. The austenite grain size was analysed by determining the mean lineal intercept and lineal intercept distribution with the aid of image analysis software. A minimum of 600 intercepts were counted for each tested condition from a minimum of 10 randomly chosen fields of view.

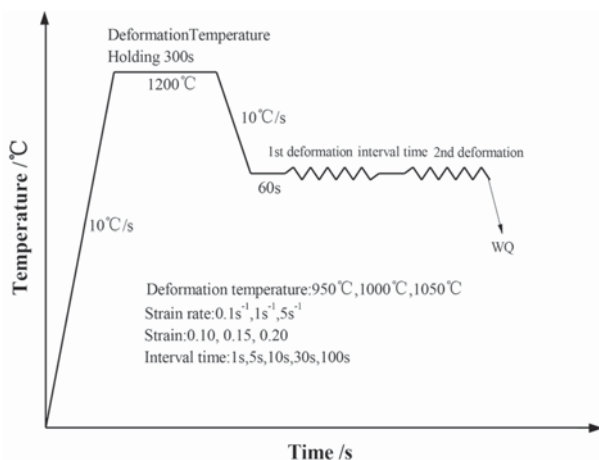


Figure 1—Schematic diagram of the hot simulation test

The interrupted hot compression tests are based on the principle that the yield stress at high temperatures is sensitive to the structural changes. The 0.2% offset yield strength was used to determine the softened fraction due to SRX and recovery (Chen, Sui, and Cui, 2014):

$$F_s = (\sigma_m - \sigma_2) / (\sigma_m - \sigma_1) \quad [1]$$

where  $\sigma_m$  is the flow stress at the interruption, and  $\sigma_1$  and  $\sigma_2$  are the 0.2% offset stresses of the first and the second compressions respectively, as shown in Figure 2.

Assuming that recrystallization starts at some critical softening fraction value, which is 0.2, the SRX fraction,  $X_s$ , can be determined from the softening data using the following formula (Miao *et al.*, 2012):

$$X_s = (F_s - 0.2) / (1 - 0.2) \quad [2]$$

## Results and discussion

To illustrate the effects of the process parameters on the SRX of Ti-Nb microalloyed high-strength steel, the stress-strain curves at different interpass times, deformation temperatures, strain rates, and strains were recorded to calculate the SRX fraction. The influence of the abovementioned variables on SRX was analysed.

### Effect of interpass time

True stress-strain curves for Ti-Nb high-strength steel deformed at a temperature of 950°C and a strain rate of 0.1 s<sup>-1</sup> are shown in Figure 3. It can be observed that by increasing the interpass time, more static softening occurred in the deformed specimen, and the second curve dropped further compared to the previous test. In other words, the yield stress of the second deformation decreases with increasing interpass time. Similar results were obtained under other test conditions. The increase in interval time allows a longer time for atomic diffusion, increasing the SRX as SRX is a thermal activation process related to atomic diffusion (Lin, Chen, and Zhong, 2008; Chen, Sui, and Cui, 2014; Mao *et al.*, 2014).

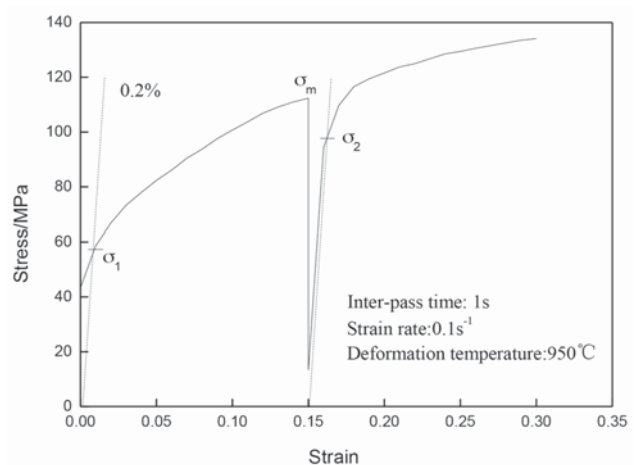


Figure 2—The true stress-strain curves of the double-hit compression test

# Static recrystallization behaviour of Ti-Nb microalloyed high-strength steel

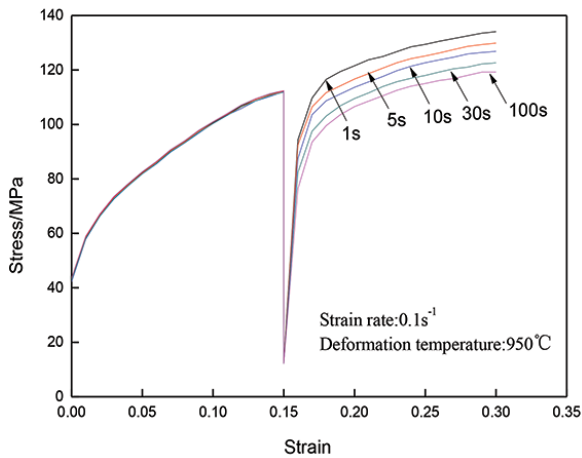


Figure 3—Flow stress curves of Ti-Nb microalloyed high-strength steel with different interpass times

## Effect of deformation temperature

Figure 4a shows the relationship between the SRX fraction and the interval time under different deformation temperatures at a strain rate of  $0.1 \text{ s}^{-1}$  and strain of 0.2. It can be seen that the softening kinetics of the specimen were accelerated by increasing the deformation temperature. Initially, the SRX fraction at a deformation temperature of  $1050^\circ\text{C}$  was higher than at  $950^\circ\text{C}$ , while the SRX fraction at  $950^\circ\text{C}$  was below 60% at the interval time of 100 seconds. This result indicates that SRX could not proceed to completion at lower temperatures, but occurred much faster at high temperature. This is due mainly to the fact that the

higher deformation-stored energy at higher temperatures accelerates SRX (Chen, Sui, and Cui, 2014). As SRX is thermally activated, the SRX fraction increases with increasing deformation temperature (Mao *et al.*, 2014).

## Effect of strain rate

The effects of strain rate on the SRX fraction were obtained at a deformation temperature of  $1000^\circ\text{C}$  and pre-strain of 0.15, as shown in Figure 4b. The softening was slightly accelerated with increasing strain rate, which indicates that strain rate had a small influence on the SRX fraction. Furthermore, the softening curve corresponding to  $0.1 \text{ s}^{-1}$  is lower than those for strain rates of  $1 \text{ s}^{-1}$  or  $5 \text{ s}^{-1}$ , especially at shorter interpass times. This is due to the higher strain energy stored in the deformed sample under high strain rate conditions (Lin, Chen, and Zhong, 2008). The reduced extent of dynamic recovery at higher strain rates results in a higher dislocation density and increases the driving force for SRX during the interpass time (Lin, Chen, and Zhong, 2008).

## Effect of pre-strain

The first deformation should be interrupted below the critical strain required for DRX. The critical strain for the start of DRX should therefore be known accurately. Generally speaking, DRX can be initiated at a critical level of stress accumulation during hot deformation. However DRX actually starts at a critical strain ( $\epsilon_c$ ) which is lower than the strain at peak stress. Only when the strain exceeds  $\epsilon_c$  does DRX occur in a hot deformation process (Ferdowsi *et al.*, 2014). The point on the flow curve at which the strain hardening rate equals zero represents the peak stress ( $\sigma_p$ ), and the inflection

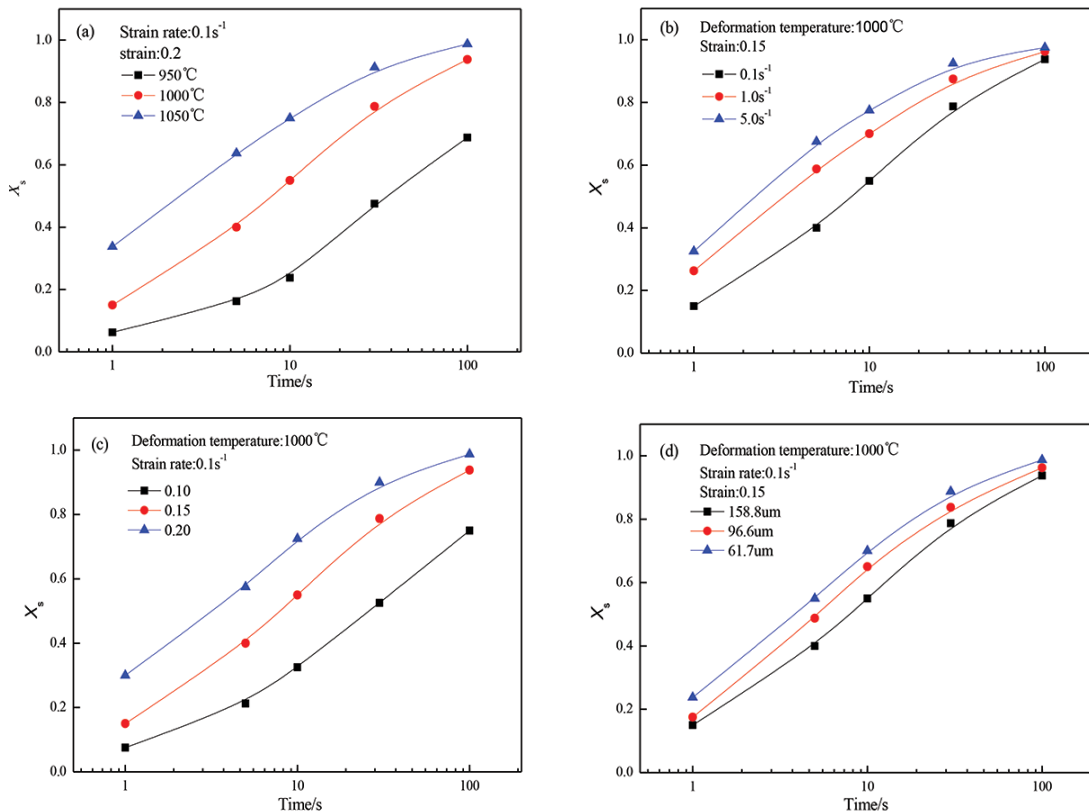


Figure 4—Static softening fraction with different process parameters: (a) deformation temperature, (b) strain rate, (c) strain, (d) initial austenite grain size

## Static recrystallization behaviour of Ti-Nb microalloyed high-strength steel

point indicates the critical stress ( $\sigma_c$ ) for the initiation of DRX. The critical strains can be determined from the inflection points of the  $\ln \theta - \varepsilon$  plots, and the critical stresses can be subsequently obtained either from the  $\theta - \sigma$  plots or from the initial flow curves (Poliak and Jonas, 2003). The relationship between  $\ln \theta$  and  $\varepsilon$  can be expressed as (Poliak and Jonas, 2003):

$$\ln \theta = A_1 \varepsilon^3 + A_2 \varepsilon^2 + A_3 \varepsilon + A_4 \quad [3]$$

where  $A_1$ ,  $A_2$ ,  $A_3$ , and  $A_4$  are constant parameters for each deformation condition. The second derivative of Equation [3] with respect to  $\varepsilon$  can be expressed as:

$$\frac{d^2 \ln \theta}{d\varepsilon^2} = 6A_1 \varepsilon + 2A_2 \quad [4]$$

At critical strain for initiation of DRX, the second derivative becomes zero. Therefore

$$\varepsilon_c = -A_2 / (3A_1) \quad [5]$$

The  $\ln \theta - \varepsilon$  curve and its corresponding third-order polynomial can yield some data. Using the flow curves, the values of peak and critical stresses and strains can be determined. The results are shown in Table I.

DRX occurs at high temperatures and low strain rates, which means the critical strain for DRX will increase with increasing strain rate at a given temperature, or increase with decreasing temperature at a constant strain rate. According to Table I, the most likely condition for DRX is 1050°C and 0.1 s<sup>-1</sup>, and the critical strain at this condition is 0.22, which is higher than the experimental conditions of strain (0.1, 0.15, and 0.2). It can therefore be concluded that DRX could not occur under the given deformation conditions.

The SRX fraction was plotted against the interval time for three pre-strains of 0.1, 0.15, and 0.2 at a strain rate of 0.1 s<sup>-1</sup> and a deformation temperature of 1000°C, as shown in Figure 4c. It can be observed that an increase in pre-strain led to an acceleration of the softening kinetics. The figure also shows that the rate of softening with a pre-strain of 0.1 was low, while the softening fraction was 75% with the interval time of 100 seconds. This means that softening under the relatively mild pre-deformation conditions resulted from recovery. However, for the higher pre-strain conditions of 0.15 and 0.20, the rate of softening was higher, which indicates that softening was caused mainly by SRX. This is due to the increase in dislocation density with pre-deformation, leading to an increase in the stored energy, thus resulting in increasing driving force for recrystallization, thereby speeding up the recrystallization process (Chen, Sui, and Cui, 2014; Mao *et al.*, 2014).

Table I Critical and peak strains at different deformation conditions			
Temperature, °C	Strain rate 0.1 s <sup>-1</sup>		
	$\varepsilon_c$	$\varepsilon_p$	$\varepsilon_c/\varepsilon_p$
950	0.25	0.35	0.71
1000	0.23	0.32	0.72
1050	0.22	0.31	0.71

### Effect of initial grain size

The deformation temperature, strain rate, and pre-strain were held constant as 1000°C, 0.1 s<sup>-1</sup>, and 0.15, respectively. The initial austenite grain sizes were 158.8, 96.6, and 61.7  $\mu\text{m}$ , respectively. The effects of the initial grain size and interval time on the SRX fractions are shown in Figure 4d. It can be observed that the softening fraction decreased with an increase in initial grain size. This is because the nucleation of SRX occurs mainly on the grain boundaries, and larger grains have less grain boundary area per unit volume, which leads to a decrease in the density of potential nucleation sites for SRX (Chen, Sui, and Cui, 2014; Lin, Chen, and Zhong, 2008).

### Modelling the kinetics of SRX

The kinetics of SRX softening can be described by an Avrami equation of the following form (Choi, 2002):

$$X_s = 1 - \exp[-0.693(\frac{t}{t_{0.5}})^n] \quad [6]$$

where  $X_s$  is the SRX fraction,  $n$  is a material-dependent constant, and  $t_{0.5}$  is the time taken to form a recrystallization volumetric fraction of 50%. The expression most widely used for  $t_{0.5}$  is (Choi, 2002):

$$t_{0.5} = A d_0^r \varepsilon^q \dot{\varepsilon}^s \exp[Q_s / (RT)] \quad [7]$$

where  $A$ ,  $r$ ,  $q$ , and  $s$  are material-dependent constants,  $\varepsilon$  is the true strain,  $\dot{\varepsilon}$  is the strain rate,  $R$  is the gas constant (Jmol<sup>-1</sup>K<sup>-1</sup>),  $T$  is the absolute temperature (K),  $Q_s$  is the activation energy of recrystallization (kJ mol<sup>-1</sup>), and  $d_0$  is the initial austenite grain size ( $\mu\text{m}$ ).

Taking the logarithm of both sides of Equation [6] twice, the following expression can be obtained:

$$\ln[\ln(\frac{1}{1-X_s})] = n \ln t - n \ln t_{0.5} + \ln 0.693 \quad [8]$$

The Avrami exponent  $n$  is obtained by linear fitting and regression analysis using a range of temperatures and pre-strains, which results in  $n = 0.58$ , under the current experimental conditions, as shown in Figure 5.

Taking the logarithm of both side of Equation [7], the following expression is obtained:

$$\ln t_{0.5} = \ln A + r \ln d_0 + q \ln \varepsilon + s \ln \dot{\varepsilon} + Q_s / (RT) \quad [9]$$

The values of  $t_{0.5}$  under different conditions can be derived from the relationships between  $X_s$  and the corresponding interval time. Then, by substituting the values of  $t_{0.5}$  and deformation temperature into Equation [9], the relationship between  $\ln t_{0.5}$  and  $10000/T$  can be obtained by linear fitting and regression analysis, as shown in Figure 6a; thus  $Q_s$  can be calculated as 326.05 kJ.mol<sup>-1</sup>. Similarly, the values of the material-dependent constants  $r$ ,  $q$ , and  $s$  are calculated as 0.86, -2.75, and -0.28 using Figures 6b, c, and d, respectively. Additionally, the constant  $A$  can be derived as  $1.37 \times 10^{-17}$  based on the obtained material-dependent constants.

Therefore the SRX kinetics for the Ti-Nb microalloyed high-strength steel can be represented as:

$$X_s = 1 - \exp[-0.693(t/t_{0.5})^{0.58}] \quad [10]$$

# Static recrystallization behaviour of Ti-Nb microalloyed high-strength steel

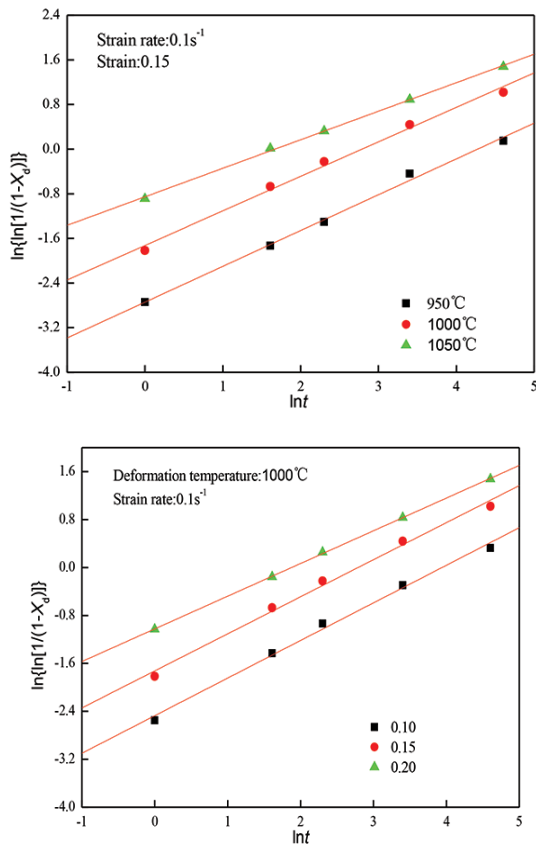


Figure 5—Relationships between  $\ln\{\ln[1/(1-X_s)]\}$  and  $\ln t$  at (a) different deformation temperatures, (b) different pre-strains

$$t_{0.5} = 1.37 \times 10^{-17} d_0^{0.86} \varepsilon^{-2.75} \dot{\varepsilon}^{-0.28} \exp[326050/(RT)] \quad [11]$$

## Comparison between experimental and predicted results

In order to verify the developed kinetic equations [10] and [11] for Ti-Nb microalloyed high-strength steel, the experimental and predicted results were compared. Figure 7 illustrates the comparisons between the experimental and predicted times for a recrystallized fraction of 50% (Figure 7a) and the recrystallization fraction under different deformation conditions (Figure 7b). The predicted and experimental results were in good agreement, indicating that the proposed kinetic equations could give a reasonable estimate of the softening behaviour during metal-forming processes.

## Conclusions

- (1) The SRX fraction of the Ti-Nb microalloyed steel increased with increasing forming temperature, pre-strain, and strain rate, and decreased with increasing initial austenitic grain size
- (2) The kinetics equations for SRX in the Ti-Nb microalloyed high-strength steel were developed to predict the softening behaviour induced by SRX, and are expressed as:

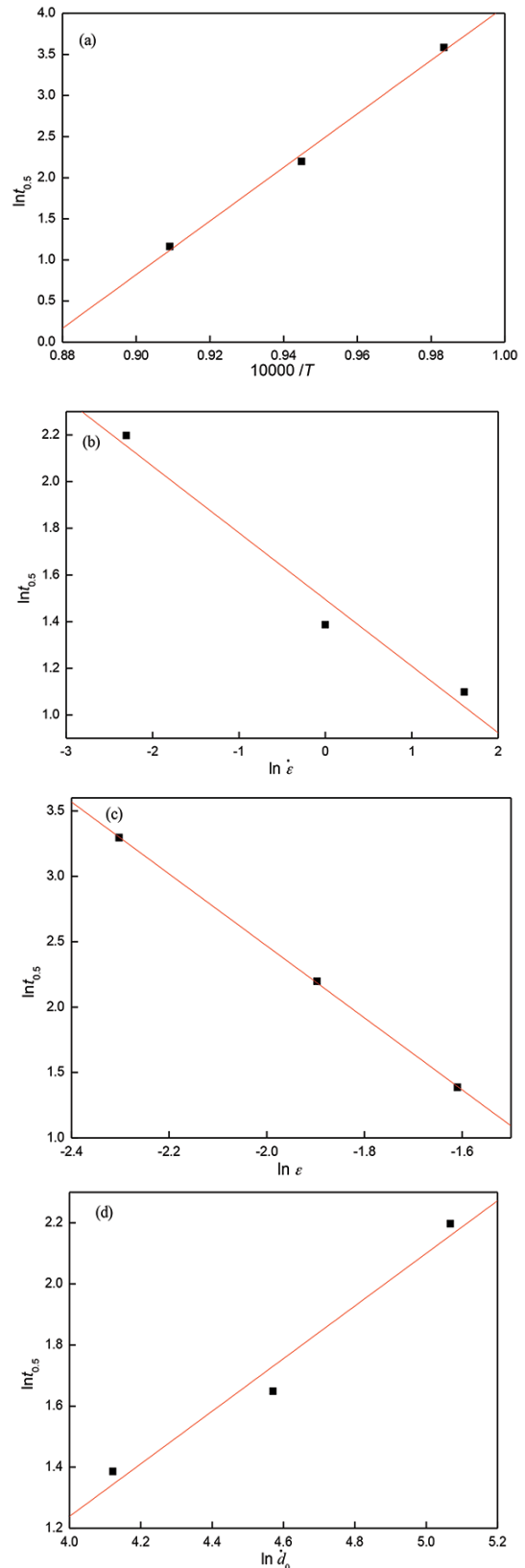


Figure 6—Relationship between  $\ln t_{0.5}$  and (a)  $10000/T$ , (b)  $\ln \varepsilon$ , (c)  $\ln \varepsilon$ , and (d)  $\ln d_0$

$$X_s = 1 - \exp[-0.693(t/t_{0.5})^{0.58}]$$

$$t_{0.5} = 1.37 \times 10^{-17} d_0^{0.86} \varepsilon^{-2.75} \dot{\varepsilon}^{-0.28} \exp[326050/(RT)]$$

## Static recrystallization behaviour of Ti-Nb microalloyed high-strength steel

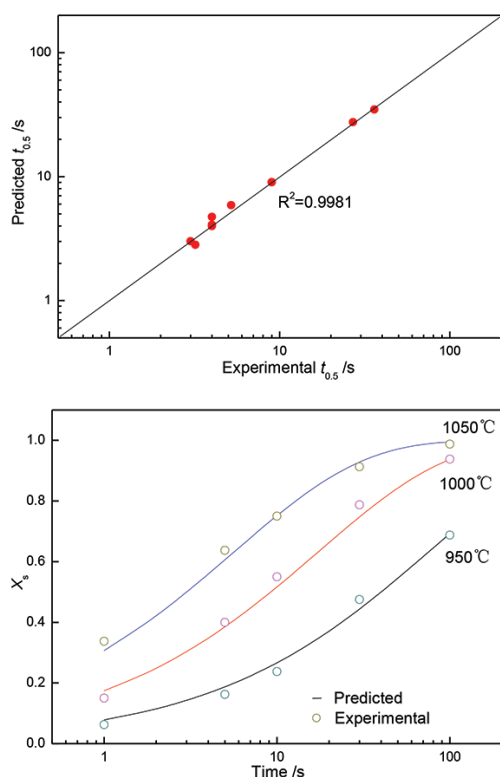


Figure 7 – Comparisons between experimental results and predicted results of (a)  $t_{0.5}$  and (b) recrystallization fraction

### References

- BANDYOPADHYAY, P.S., KUNDU, S., GHOSH, S.K., and CHATTERJEE, S. 2011. Structure and properties of a low-carbon microalloyed ultra-high-strength steel. *Metallurgical and Materials Transactions A*, vol. 42, no. 4. pp. 1051–1061.
- CABRERA, J.M., OMAR, A.A., PRADO, J.M., and JONAS, J.J. 1997. Modeling the flow behavior of a medium carbon microalloyed steel under hot working conditions. *Metallurgical and Materials Transactions A*, vol. 28, no. 11. pp. 2233–2244.
- CHEN, B.H. and YU, H. 2012. Hot ductility behavior of V-N and V-Nb microalloyed steels. *International Journal of Minerals, Metallurgy and Materials*, vol. 19, no. 6. pp. 525–529.
- CHEN, F., SUI, D.S., and CUI, Z.S. 2014. Static recrystallization of 30Cr2Ni4MoV ultra-super-critical rotor steel. *Journal of Materials Engineering and Performance*, vol. 23, no. 8. pp. 3034–3041.
- CHEN, J., LV, M.Y., TANG, S., LIU, Z.Y., and WANG, G.D. 2015. Influence of thermomechanical control process on the evolution of austenite grain size in a low-carbon Nb-Ti-bearing bainitic steel. *Journal of Materials Engineering and Performance*, vol. 24, no. 10. pp. 3852–3861.
- FERDOWSI, M.R.G., NAKHAIE, D., BENHANGI, P.H., and EBRAHIMI, G.R. 2014. Modeling the high temperature flow behavior and dynamic recrystallization kinetics of a medium carbon microalloyed steel. *Journal of Materials Engineering and Performance*, vol. 23, no. 3. pp. 1077–1087.
- LIANG, H.Q., NAN, Y., NING, Y.Q., LI, H., ZHANG, J.L., SHI, Z.F., and GUO, H.Z. 2015. Correlation between strain-rate sensitivity and dynamic softening behavior during hot processing. *Journal of Alloys and Compounds*, vol. 632. pp. 478–485.
- LIN, Y.C., CHEN, M.S., and ZHONG, J. 2008. Study of static recrystallization kinetics in a low alloy steel. *Computational Materials Science*, vol. 44, no. 2. pp. 316–321.
- MAO, H.J., ZHANG, R., HUA, L., and YIN, F. 2014. Study of static recrystallization behaviors of GCr15 steel under two-pass hot compression deformation. *Journal of Materials Engineering and Performance*, vol. 24, no. 2. pp. 930–935.
- MIAO, C.L., SHANG, C.J., ZUROB, H.S., ZHANG, G.D., and SUBRAMANIAN, S.V. 2012. Recrystallization, precipitation behaviors, and refinement of austenite grains in high Mn, high Nb steel. *Metallurgical and Materials Transactions A*, vol. 43, no. 2. pp. 665–676.
- MIRZADEH, H., CABRERA, J.M., and NAJAFIZADEH, A. 2012. Modeling and prediction of hot deformation flow curves. *Metallurgical and Materials Transactions A*, vol. 43, no. 1. pp. 108–123.
- OPIELA, M. 2014. Effect of thermomechanical processing on the microstructure and mechanical properties of Nb-Ti-V microalloyed steel. *Journal of Materials Engineering and Performance*, vol. 23, no. 9. pp. 3379–3388.
- POLIAK, E.I. and JONAS, J.J. 2003. Initiation of dynamic recrystallization in constant strain rate hot deformation. *ISIJ International*, vol. 43, no. 5. pp. 684–691.
- SANGWOO, C. and YOUNGSEOG, L. 2002. A new approach to predicting partial recrystallization in the multi-pass hot rolling process. *Metals and Materials International*, vol. 8, no. 1. pp. 15–23.
- SHUKLA, R., DAS, S.K., RAVIKUMAR, B., GHOSH, S.K., KUNDU, S., and CHATTERJEE, S. 2012. An ultra-low carbon, thermomechanically controlled processed microalloyed steel: microstructure and mechanical properties. *Metallurgical and Materials Transactions A*, vol. 43, no. 12. pp. 4835–4845.
- SICILIANO, F. and JONAS, J.J. 2012. Mathematical modeling of the hot strip rolling of microalloyed Nb, multiply-alloyed Cr-Mo, and plain C-Mn steels. *Metallurgical and Materials Transactions A*, vol. 31, no. 2. pp. 511–530.
- WU, L.Z., LI, X.S., CHEN, J., ZHANG, H.B., and CUI, Z.S. 2010. Dynamic recrystallization behavior and microstructural evolution in SPHC steel. *Journal of Shanghai Jiaotong University (Science)*, vol. 15, no. 3. pp. 301–306.
- ZHANG, W.F., SHA, W., YAN, W., WANG, W., SHAN, Y.Y., and KE, Y. 2014. Constitutive modeling, microstructure evolution, and processing map for a nitride-strengthened heat-resistant steel. *Journal of Materials Engineering and Performance*, vol. 23, no. 8. pp. 3042–3050. ◆